Available online at www.sciencedirect.com
SCIENCE DIRECT®
Journal of Hydrology 282 (2003) 145–163
Journal of Hydrology
www.elsevier.com/locate/jhydrol

Modelling changes in the mass balance of glaciers of the northern hemisphere for a transient $2 \times CO_2$ scenario

Christian Schneeberger[a], Heinz Blatter[a], Ayako Abe-Ouchi[b], Martin Wild[a,*]

[a]*Institute for Atmospheric and Climate Science, Swiss Federal Institute of Technology, Winterthurerstrasse 190, CH-8057 Zürich, Switzerland*
[b]*Center for Climate System Research, University of Tokyo, 4-6-1 Komaba, Meguro-ku, Tokyo 153, Japan*

Abstract

A climate forecast provided by a General Circulation Model (GCM), a glacier mass balance model and a glacier flow model is applied to a sample of 11 small glaciers. Another sample of six glaciers and six large, heavily glacierized areas in the arctic were modelled using only the climate forecast and the glacier mass balance model.

The climate forecast of two different GCM's with identical experimental setup takes into account a gradual increase in atmospheric content of CO_2 and other greenhouse gases to a doubled CO_2 equivalent in 2050 corresponding to the IPCC Scenario IS92a. The differences between the two GCM's are significant for the future development of the glacierization of arctic areas.

The glacier mass balance model consists of a temperature index melt model, which uses potential direct clear sky radiation to obtain a better spatial and temporal resolution, combined with imposed snow precipitation. Static mass balance sensitivities span -0.2 to -1.5 mwe a^{-1} °C, the higher and lower sensitivities apply for glaciers in more maritime and continental climates, respectively. All of the modelled glaciers and glacierized regions show a strong decrease in the net mass balance. Temperature changes dominate the effect of snow precipitation on the net mass balance. A temperature increase results in substantial increase in melt especially through the extension of the melt season in spring and fall. The mass balance projections for the sample of 11 glaciers are then used in a glacier flow model to simulate the dynamic reaction of the glacier to the changing climatic conditions. An iteration procedure accounts for possible feedback of changes in the glacier area and the ice surface elevation to the projected mass balance.

For the modelled glaciers, an average volume loss of 60% until 2050 is predicted. Without the above iteration and assuming a constant glacier area, the volume change is overestimated by about 20%. A comparison with the climate predictions of the two different GCMs shows only a difference of about 10% in the mass loss obtained by flow modelling of four glaciers.

Keywords: Glacier; Climate change; Mass balance; Ice volume

1. Introduction

Mountain glaciers play an important role in the water budget of many regions in the world. The storage of snow and ice in their upper parts and summer melt in the lower parts strongly determines the seasonal runoff pattern of glacierized regions. Especially in areas with dry summer seasons, glacier runoff may be the only substantial source of water during this season. For planning purposes it may thus be crucial to know the future evolution of the mass budgets and correspondingly, the evolution of the surface and ice mass of the glaciers. Furthermore,

* Corresponding author. Tel.: +41-1-635-5221; fax: +41-1-362-5197.
E-mail address: blatter@iac.umnw.ethz.ch (H. Blatter).

0022-1694/$ - see front matter © 2003 Elsevier B.V. All rights reserved.
doi:10.1016/S0022-1694(03)00260-9

since smaller glaciers react on short time scales their contribution to sea level changes may exceed those of the large ice sheet in the near future.

To project the evolution of a glacier, a prediction of the future mass budget is necessary. The mass budget, however, is a composite quantity which depends in complex ways on climate elements and their seasonal patterns. One way to achieve this goal is a combined numerical modelling of the involved processes. In this work, three numerical models are used, (1) an Atmosphere–Ocean General Circulation Model (AO-GCM) to simulate the climatic conditions corresponding to some greenhouse scenario, (2) a model to compute the surface mass balance on a glacier based on climatic input, and (3) an ice flow model to predict the evolution of the glacier surface for a given mass balance scenario.

The climate scenario are computed with GCM's based on the IPCC scenario IS92a (IPCC, 1990). This scenario predicts a doubling of the atmospheric CO_2 concentration in the year 2050 with respect to the preindustrial value. To compute the present mass balance of the glacier the present day observed climate was used. To obtain a climate scenario for the local situation on the glacier for the year 2050, the modelled climate change between today and 2050 for a representative GCM grid point is added to the present day observed climate.

This procedure is applied to a sample of glaciers, selected on the base of availability of comprehensive glaciological data. A similar approach was used to model larger, heavily glacierized regions. Assuming that the information obtained from one single glacier is valid for an entire area or for similar climatic settings, the mass balance modelling can be done for such larger areas. These larger areas are also selected based on available mass balance estimates on individual local glaciers, for which the mass balance model was tuned.

A detailed description of the method applied to Storglaciaeren, Sweden, is given in Schneeberger et al. (2001).

2. The models

2.1. The GCM time slice experiments

The models used in this study are the ECHAM4 GCM of the Max-Planck-Institute for Meteorology (Roeckner et al., 1996; Roeckner et al., 1999) and the Center for Climate System Research/National Institute of Earth Sciences (CCSR/NIES) GCM (Emori et al., 1999). A 'time-slice' method was adopted (Cubasch et al., 1995; Wild et al., 1997).

In the framework of the EU Project SIDDACLICH (SImulation, Detection and Diagnosis of Anthropogenic CLImate CHange) (Cubasch et al., 1997), climate change scenarios of unprecedented high resolution were performed. The aim was to obtain scenarios at the highest horizontal resolution currently used in climate modelling: 1.1° (T106). This was motivated by the fact that an increase in horizontal resolution up to this magnitude results in an improved simulation of the precipitation fields, particularly in areas where orography-induced precipitation is dominant, such as over the polar ice sheets (Ohmura et al., 1996; Wild et al., 2003). Precipitation is also predominantly orography-induced in the area considered in this study.

Since it was not feasible to run such a high resolution GCM over several decades with the available supercomputing resources, as required in transient climate change experiments, a 'time-slice' method was adopted (Cubasch et al., 1995; Wild et al., 1997). Thereby the high resolution atmospheric model is run at the time where the CO_2 concentration is expected to double, using prescribed boundary conditions of sea surface temperature and sea ice distribution, which are derived from a lower resolution, transient coupled atmosphere–ocean scenario run. Specifically, T106 ($\approx 1.1°$) experiments with ECHAM4 were carried out for both present day and $2 \times CO_2$ conditions with associated sea surface temperature and sea-ice distributions derived from a transient scenario run with ECHAM4 at T42 ($\approx 2.8°$) resolution coupled to the OPYC ocean model (Roeckner et al., 1999). This scenario run takes into account a gradual increase in CO_2 and other greenhouse gases according to the IPCC Scenario IS92a (IPCC, 1990). The T106 experiment for present day conditions uses the Atmospheric Model Intercomparison Project (AMIP) Sea Surface Temperature (SST) climatology (Gates, 1992), superimposed with detrended SST variabilities from the coupled T42 experiment, representative for the decade 1971–1980. The experiment under $2 \times CO_2$ conditions is representative for the decade 2041–2050 and uses the SST

obtained through a superposition of the AMIP SST climatology with the mean SST changes between the periods 1971–1980 and 2041–2050 and the SST variabilities for 2041–2050, both taken from the coupled T42 experiment.

'Time-slice' Experiments with the CCSR/NIES GCM with T106 resolution were carried out for both present day and $2 \times CO_2$ conditions with associated sea surface temperature and sea ice distributions derived from a transient scenario with CCSR/NIES atmospheric GCM at T21 ($\approx 5.6 \times 5.6°$) resolution coupled to CCSR OGCM1 at $2.8 \times 2.8°$ resolution (Emori et al., 1999). The scenario runs take into account a gradual increase in CO_2 and other greenhouse gases according to the IPCC Scenario IS92a (IPCC, 1990). In this text we will refer to the present day situation as CTRL and to the $2 \times CO_2$-state as $2 \times CO_2$.

2.2. The glacier mass balance model

A grid-based (distributed) mass balance model based on the melt model of Hock (1999) is used to calculate accumulation and ablation on the glacier based on air temperature, precipitation and potential direct solar radiation. Computations are performed for each grid cell of digital elevation models with different horizontal resolution ($50 \times 50\ m^2$–$200 \times 200\ m^2$). The air temperature is extrapolated to all grid cells using a constant lapse rate that was determined by tuning the altitudinal distribution of modelled mass balance to the measured mass balance. The range of possible lapse rates was limited to a range within observed evidence.

Precipitation P is assumed to increase linearly with elevation z, up to an elevation above which saturation occurs (z_s)

$$P(z) = P_0 + sP_0(z_s - z_0), \tag{1}$$

where z_0 is the altitude of the precipitation measurement, P_0 is the prescribed precipitation at a given time and sP_0 is the precipitation lapse rate. Above the saturation elevation (z_s) precipitation is assumed to remain constant. Again, the values of both the altitudinal precipitation gradient and the maximum precipitation elevation were used for tuning modelled mass balance to measured values. Accumulation is computed from precipitation using a fixed air temperature divider of 1.5 °C to determine whether or not precipitation falls as snow. A mixture of rain and snow is assumed for a transition zone ranging from 1 K above and 1 K below the threshold temperature with linear interpolation of the percentages of snow and rain in between.

Ice and snow melt rates M are computed from a temperature index model including potential direct solar radiation at the surface, I_{pot}, and only requiring air temperature T as climatic input data (Hock, 1999). I_{pot} is calculated as a function of top of atmosphere solar radiation, an assumed atmospheric transmissivity, solar geometry and topographic characteristics (Garnier and Ohmura, 1968). If the grid cell considered is shaded by surrounding topography, I_{pot} is set to zero. The melt rate is

$$M = \begin{cases} (F_m + r_{snow/ice} I_{pot})T & \text{if } T > 0\ °C, \\ 0 & \text{if } T \leq 0\ °C, \end{cases} \tag{2}$$

where F_m is a melt factor, $r_{snow/ice}$ is a radiation coefficient which differs for snow and ice surfaces. The melt factor and the radiation coefficients are empirical coefficients which are applied to the whole glacier. This also justifies the application of an averaged free atmosphere temperature lapse rate to determine the near glacier air temperature rather than the local temperature on the ice surface, which is strongly influenced by the glacier itself. The values of the used parameters are listed in Table 1 for all chosen glaciers and glacierized regions.

Since the used glacier melt model is a temperature index melt model, the air temperature representative of the surrounding region is required rather than the local air temperature close to the glacier surface. This is true because of the fact that glacier melt is determined to a high degree by the incoming longwave radiation, which in turn is determined to a high degree by the atmospheric temperature in the lowest 1000 m above the surface (Ohmura, 2001). This indicates the physical basis for the high correlation between atmospheric temperature and ice melt, and it explains why temperature index melt models work relatively well. The use of potential direct radiation improves temporal and spatial information without the need for additional data.

Table 1
Parameters for the mass balance model for each glacier

Glacier	Location	F_m (10^{-4} m s^{-1} K^{-1})	r_{snow} (10^{-10} m^3 s^{-1} W^{-1} K^{-1})	r_{ice} (10^{-10} m^3 s^{-1} W^{-1} K^{-1})	dT/dz (10^{-2} °C/m)	s (10^{-4} m^{-1})
1 Arolla	Alps	1.67	7.39	7.33	−0.6	10
2 Gries	Alps	1.67	6.56	6.56	−0.7	40
3 Stor	Scandinavia	1.67	6.64	7.19	−0.7	40
4 Enga	Scandinavia	0.50	2.78	2.05	−0.1	15
5 Dzhankuat	Russia	1.42	5.00	5.13	−0.5	8
6 Obruchev	Kaukasus	0.84	3.33	3.59	−0.9	25
7 Abramov	Kirghistan	1.42	5.00	5.13	−0.5	20
8 No. 1	Tien Shan	0.17	2.22	2.56	−0.72	5
9 Aktru	Russia	0.84	3.89	4.10	−0.8	20
10 Shumsky	Kazakhstan	0.63	1.11	1.54	−0.5	15
11 No. 31	Siberia	2.92	16.11	14.36	−0.9	5
12 Wolverine	Alaska	3.76	18.53	17.61	−0.5	25
13 Gulkana	Alaska	0.65	2.97	3.26	−0.7	40
14 S. Cascade	NW-USA	0.76	2.17	2.51	−0.75	40
15 M. Lovén	Svalbard	2.51	10.56	10.25	−0.7	10
16 A. Brøgger	Svalbard	2.51	11.81	11.41	−0.7	10
17 Lewis	Kenya	0.84	2.72	3.03	−0.7	5
Region	Location	F_m (10^{-4} m s^{-1} K^{-1})	r_{snow}	r_{ice} (10^{-10} m^3 s^{-1} W^{-1} K^{-1})	dT/dz (10^{-2} °C/m)	s (10^{-4} m^{-1})
A Baffin Isl.	Can. Arctic	2.09	12.20	11.77	−0.6	10
B Ellesmere Isl.	Can. Arctic	1.67	7.50	7.43	−0.5	10
C Svalbard	Europ. Arctic	3.76	25.00	23.59	−0.7	10
D Franz Josef	Russ. Arctic	0.42	1.42	1.82	−0.9	25
E Nov. Zeml.	Russ. Arctic	0.84	3.33	3.59	−0.9	25
F Zev. Zeml.	Russ. Arctic	0.84	3.33	3.59	−0.9	15

2.3. The glacier model

A glacier model based on an ice flow model and a mass balance scenario was used to compute the evolution of the glaciers. The flow model solves the mass and force balance equations for a three-dimensional ice mass with given surface and basal topography. It includes the normal deviatoric stress gradients and the lateral shear stresses, and handles a non-linear stress–strain relation to calculate stress and velocity fields with given surface and basal boundary conditions (Blatter, 1995; Colinge and Blatter, 1998).

The surface evolution code computes the mass flux gradients using the above velocity components and then determines the surface change and margin migration corresponding to the imposed surface mass flux distribution for a time step (Albrecht, 1999). The model considers a two-dimensionally distributed surface mass flux.

2.4. Local climate

The basic hypothesis for the use of the GCM climate predictions for making local climate predictions is, that while mean values of temperature and precipitation change, spatial gradients are affected to a much smaller extent. According to this assumption, the changes in climatic elements representative of a larger area (100 km) are, to a high degree, also representative for the changes of the local climate. The reduction of available climate input to the local conditions on the glacier is based on observations of the present climate and the differences between corresponding modelled temperature and precipitation values for present time and 2050. Therefore, only these differences are relevant for this study, and not the absolute values of the time slice runs.

The annual cycle of temperature, necessary for the simulation with the melt/accumulation model, was

constructed by linearly interpolating climatic monthly mean values obtained from measurements from nearby climate stations. In addition to the annual cycle, daily temperature cycles (and their changes based on the GCM simulations) were implemented based on maximum/minimum temperatures. For the $2 \times CO_2$ run of the melt/accumulation model, changes in daily temperature as well as of the diurnal cycle were added to the CTRL implementation.

For the control run, precipitation events were generated randomly while conserving the observed seasonal totals and an observed upper limit of the amount of precipitation in one event. For the $2 \times CO_2$ run of the melt/accumulation model, the percentual changes between GCM control and $2 \times CO_2$ precipitation were added to the above-mentioned randomly generated precipitation events.

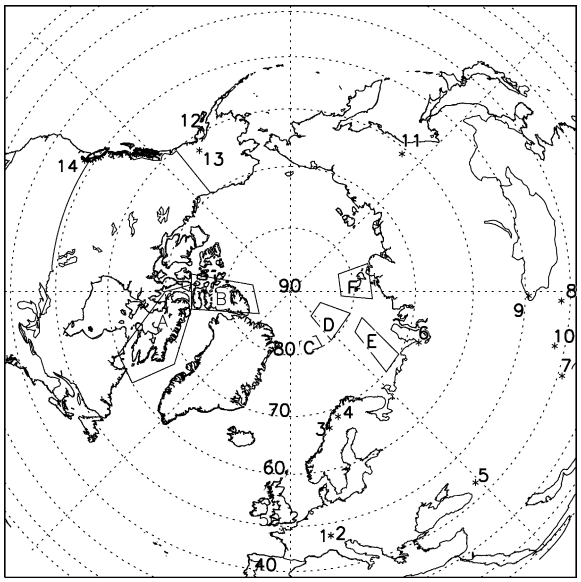

Fig. 1. Distribution of the selected glaciers. Numbers correspond with the ones from Table 1. The letters designate larger, heavily glaciated areas, that were used for mass balance modelling (Table 2). Lewis Glacier (Kenya, 17) is located outside of the map range, just a little north of the equator. Austre Brøggerbreen (16) and Midre Lovénbreen (15) are situated in Svalbard (C), but are omitted for clarity.

3. Case studies

A total number of 17 glaciers of the northern hemisphere and equatorial regions, for which sufficient information is available, were selected for this study (Fig. 1). These glaciers are located in different climatic situations, from high latitudes to the equator and from extreme maritime to extreme continental climates. Most of these glaciers are small, i.e. less than 5 km long and volumes smaller than 10^9 m^3, and thus, their response times are a few decades at most (Johannesson et al., 1989). For 11 out of the 17 glaciers, the whole method including the glacier dynamic modelling was applied. For the other six glaciers, some of the necessary information was missing, and the application of the glacier flow model was not warranted.

In the following, a short description of each glacier is given. The main source of mass balance measurements are the Fluctuation of Glaciers (IASH(ICSI)-UNESCO, 1967, 1973, 1977, 1985, 1988, 1993a, 1998) and the Glacier Mass Balance Bulletin (IASH(ICSI)-UNESCO, 1991, 1993b, 1994, 1996, 1999). If not otherwise stated, these publications were used as source for mass balance information.

The bed of *Haut Glacier d'Arolla*, Swiss Alps, was radar sounded in 1989 and 1990 (Sharp et al., 1993) and ablation data is available for the years 1989–1991 (M. Sharp, personal communication, September 1993). Measured spatial and temporal variations of surface ice velocities and vertical velocity profiles were used to validate the ice flow model and test basal sliding scenarios (Hubbard et al., 1998).

Griesgletscher, Swiss Alps, was investigated extensively since the 1950s during the planning of a dam. Measurements of mass balance began in 1961 (Funk et al., 1997) and there is detailed information on surface velocities (Kääb, 1996), and maps of the ice surface in 1961, 1979, 1986 and 1991 (Aellen and Funk, 1988) and basal topography (Vieli, 1996) are available. The glacier flow model was validated with the observed information on Griesgletscher (Albrecht, 1999).

The method presented in this work was developed and tested with the information available on *Storglaciaeren*, northern Sweden (Schneeberger et al., 2001). The maps of mass balance distribution (Holmlund and Jansson, 1999) and ice surface maps of 1959, 1969, 1980 and 1990 (Holmlund, 1996) were used to test the ice and snow melt model of Hock (1999) based on

the weather record made during the same period at the Tarfala Research Station, and the glacier model of Albrecht (1999) and Albrecht et al. (2000).

Data on *Engabreen* (an outlet glacier from the Svartisen Ice Cap) is published every year by the Norges Vassdrags- og Energidirektorat (NVE) in its report series (Kjøllmoen, 2000). It is the largest glacier in this study with a surface area of 38 km^2. Mass balance measurements began in 1970 and the glacier surface was mapped in 1968. Engabreen is currently experiencing a phase of strong advance caused by positive mass balance of a number of years. This is rather typical for the state of the Norwegian glaciers located in the maritime climate.

Dzhankuat is a valley-type glacier, located on the northern slope of the central part of the Main Caucasus Ridge. A long series of mass balance measurements is available, and the glacier has been mapped in 1968, 1974, 1984, 1992 and 1996 (Moscow State University, unpublished).

Obruchev is a small valley glacier (area 0.3 km^2, length 1 km) situated in the Polar Urals. It is characterized by its low setting with an altitude range of 390–660 m a.s.l. and a mean equilibrium line altitude (ELA) of 530 m. Mass balance measurements exist since 1960 and are published in Jania and Hagen (1996).

Abramov glacier is a glacier in the Alay Range of Kirghizstan. It has been studied in detail since 1967. However, the Glaciological Research Station has recently been destroyed by rebells, so that this valuable source of climatological and glaciological information is in danger. All available information has been published in Pertziger (1996).

Urumqi South *Glacier No. 1* is situated in the Chinese Tian Shan Mountains. It consists of two branches, no longer connected to each other. It is a predominantly cold glacier, but reaches melting temperatures over wide areas of the bed. Long term measurements of both mass balance and meteorological elements are available (Chaohai and Tianding, 1992; Cao, 1998). The glacier bed was radar sounded in 1982 (Zhang et al., 1985).

Aktru is an area in the Russian Altai Mountains with several glaciers, the most famous amongst them the Maliy Aktru. A long time (1970-present) series of mass balance measurements exists for Maliy Aktru. Using the information on ELA this information was extended to the other glaciers in that area by assuming a constant ELA, an assumption that is supported by the data published in the Glacier Mass Balance Bulletins.

Shumsky Glacier of the Dzhungarian Alatau Range has been chosen as a sample for a larger set of glaciers in this area, due to its representative elevation, orientation, steepness, and morphological setting (Cherkasov et al., 1996). There is a mass balance record for the period 1967–1991 from a network of 200 stakes, as well as mappings of the ice surface topography and ice thickness in 1984 (Cherkasov and Nikitin, 1989). According to Cherkasov et al. (1996) the glacier was loosing mass during the observation period.

Glacier *No. 31* is situated in the Suntar-Khayata Ridge in Eastern Siberia. Glaciological information stems from field experiments in 1957–1959. Basal topography was sounded only for the lower part of the glacier (Kotlyakov, 1997).

Wolverine glacier is one of the three 'USGS benchmark glaciers'. They are monitored in great detail, because they are assumed to be representative for the area and the climatic setting they are situated in. For Wolverine Glacier, no basal topography measurements exist. Wolverine Glacier lies on the Kenai Peninsula close to the Pacific and thus receives a large amount of precipitation, but the temperatures are less extreme than further inland (maritime climate). According to Hodge et al. (1998), its mass balance is highly correlated with South Cascade glacier, another one of the Benchmark glaciers, further south in the USA.

Gulkana glacier is the second of the three 'USGS benchmark glaciers'. Gulkana glacier experiences a continental climate, since it is shaded from the pacific moisture source by the Alaska Range. Few radar soundings are not covering the whole glacier (Ostenson et al., 1965; March, 2000). Mass balance data is available for the period 1965–1990.

South Cascade is the third of the 'USGS benchmark glaciers'. Situated in the Cascade Mountains (WA, USA). South Cascade Glacier gets a considerable amount of precipitation, although it is somewhat shielded from the main storm track by the Olympic Mountains on the Olympic Peninsula. Temperatures are rather warm throughout the year. Detailed information on mass balance and runoff and some

information on the velocity is available, as well as a long record (1962 to present) of climatic measurements near the glacier. The bed of South Cascade glacier was radar sounded in 1990–1994 (Fountain and Jacobel, 1997).

Long term mass balance measurements (1967–88) exist for both *Midtre Lovénbreen* and *Austre Brøggerbreen* (Hagen and Liestøl, 1990). These measurements show strongly negative balances for both glaciers for this period.

Detailed information on *Lewis* Glacier is given by Hastenrath (1996). Lewis glacier is currently experiencing a phase of strong retreat and is likely to disappear in the near future even under current climatic conditions.

In addition to modelling the single glaciers, a similar approach was used to model larger, heavily glaciated areas. Assuming that the information obtained from the single glacier is valid for an entire area or for similar climatic settings, the mass balance modelling can be done for such larger areas. These larger areas are selected based on available mass balance estimates (Dowdeswell et al., 1997) to which the mass balance model was tuned using additional information from single glaciers.

Baffin Island has a glacierized area of about 37,000 km^2 (Haeberli et al., 1989). There is a number of mass balance measurements, but most of them are discontinuous, the longest being the one from the Barnes Ice Cap (1963–1984).

The *Queen Elisabeth Islands* consist of Ellesmere Island, Coburg Island, Axel Heiberg Island, Melville Island, Meighen Island and Devon Island. This results in a total of almost 125,000 km^2 of ice-covered area (Dowdeswell et al., 1997). For this area, a number of discontinuous and continuous long term mass balance time series are available, especially on Axel Heisberg Island (White Glacier, 1959-present), but also on the other Islands (e.g. Gilman Glacier and Agassiz Ice Cap on Ellesmere Island or Laika Glacier on Coburg Island) (Jania and Hagen, 1996).

Svalbard is an archipelago of a total area of 61,680 km^2 with an estimated glacier area of 36,589 km^2 (59%). It has a variety of small and medium-sized glaciers and the total ice volume is estimated at 11,000 km^3 (Jania and Hagen, 1996). Its northern location in junction with the large heat transport trough the Norwegian Sea makes it susceptible to climatic changes. The warming at the beginning of the 20th century strongly affected glacier mass balances and initiated a retreat of calving fronts. The first systematic mass balance measurements in Svalbard were initiated by the Norsk Polar Institute (NPI) in 1950 on Finsterwaldbreen, followed by several monitoring programs on different glaciers.

Franz Josef Land is an archipelago with a total area of 16,134 km^2 and a glacierized area of 13,735 km^2 (81.5%), and its highest point is at 735 m a.s.l. The total volume of ice is estimated to be 2500 km^3 (Jania and Hagen, 1996).

Novaya Zemlya consists of two large and a number of smaller islands. The area is about 81,270 km^2 with a glacierization of about 29.1% (23,645 km^2). The estimated total ice volume is about 9500 km^3. Mass balance measurements are scarce and incomplete (Jania and Hagen, 1996).

Four main islands together with a number of smaller ones form the archipelago of *Severnaya Zemlya*. It is the northernmost archipelago in Asia and was discovered as late as in 1913. The total area is about 36,788 km^2 with a glacierized area of about 18,326 km^2 (49.8%). The total volume is estimated to be 5500 km^3. The highest point is at 965 m a.s.l. (Jania and Hagen, 1996).

4. Results

4.1. Climate prediction

From both the ECHAM and CCSR AO-GCM time slice experiments, near surface air temperatures and precipitation were extracted for the nearest gridpoints of the chosen glaciers. The ECHAM experiment provides the six hourly and the daily maximum and minimum temperatures, from the CCSR experiment the monthly mean values were taken. The monthly mean air temperatures and the monthly total precipitation at the gridpoints representative for the 17 glaciers and 6 glacierized areas listed in Section 3 (Fig. 1) are shown in Fig. 2 for both climate forecasts. The temperature curves are not applicable to the elevation of the glaciers directly, but they are representative for the surrounding area. Since the downscaling is based on the assumption that the changes in the climate elements is also representative

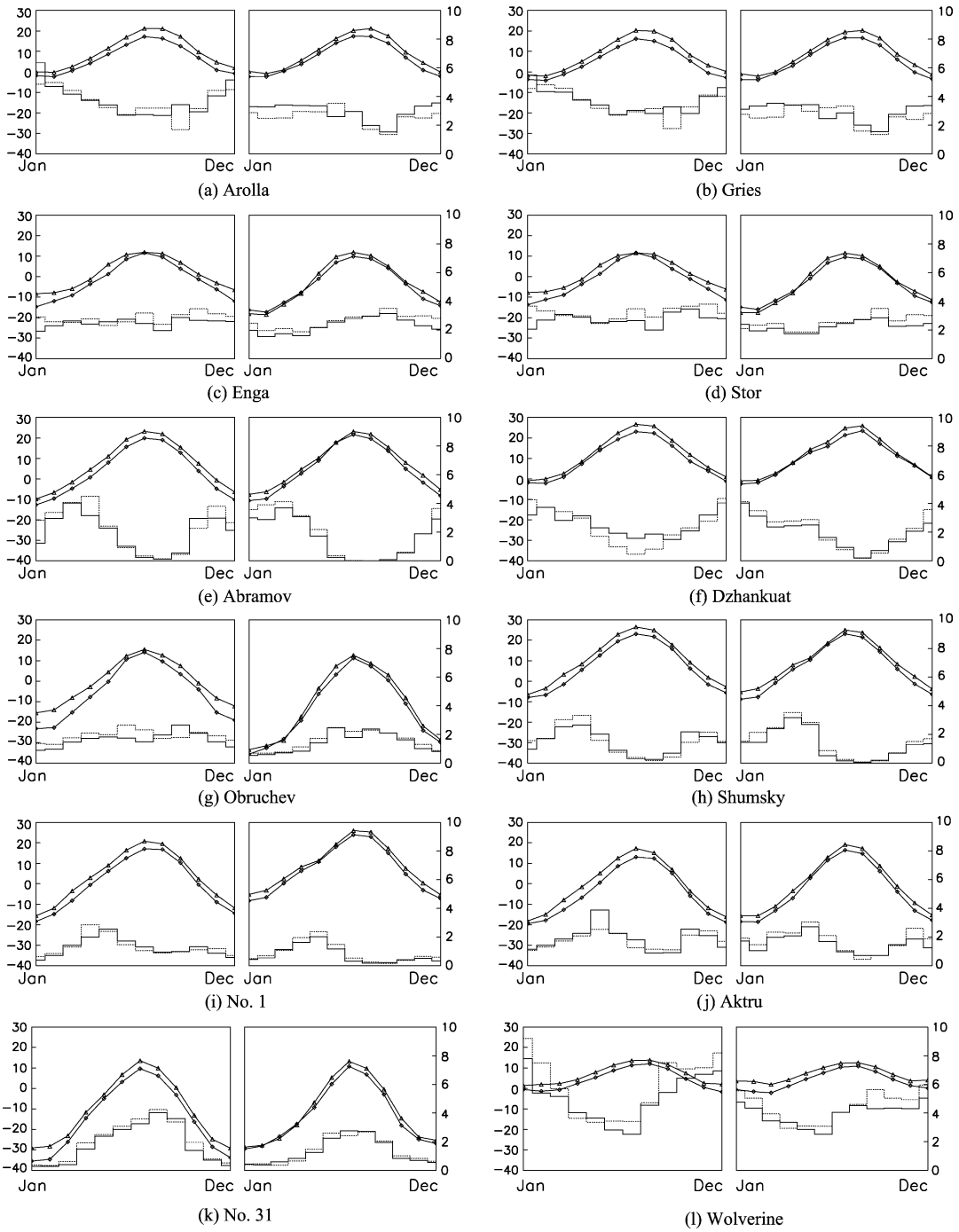

Fig. 2. Comparison between the ECHAM and CCSR climate scenarios for the gridpoints closest to the corresponding glaciers (or areas). The left panel shows the data for the ECHAM model and the right panel the same information from the CCSR. Diamonds are CTRL temperatures while triangles are $2 \times CO_2$ temperatures (°C), the bar plot (solid line) shows precipitation (mm/day) for the CTRL and the dotted line for the $2 \times CO_2$ conditions.

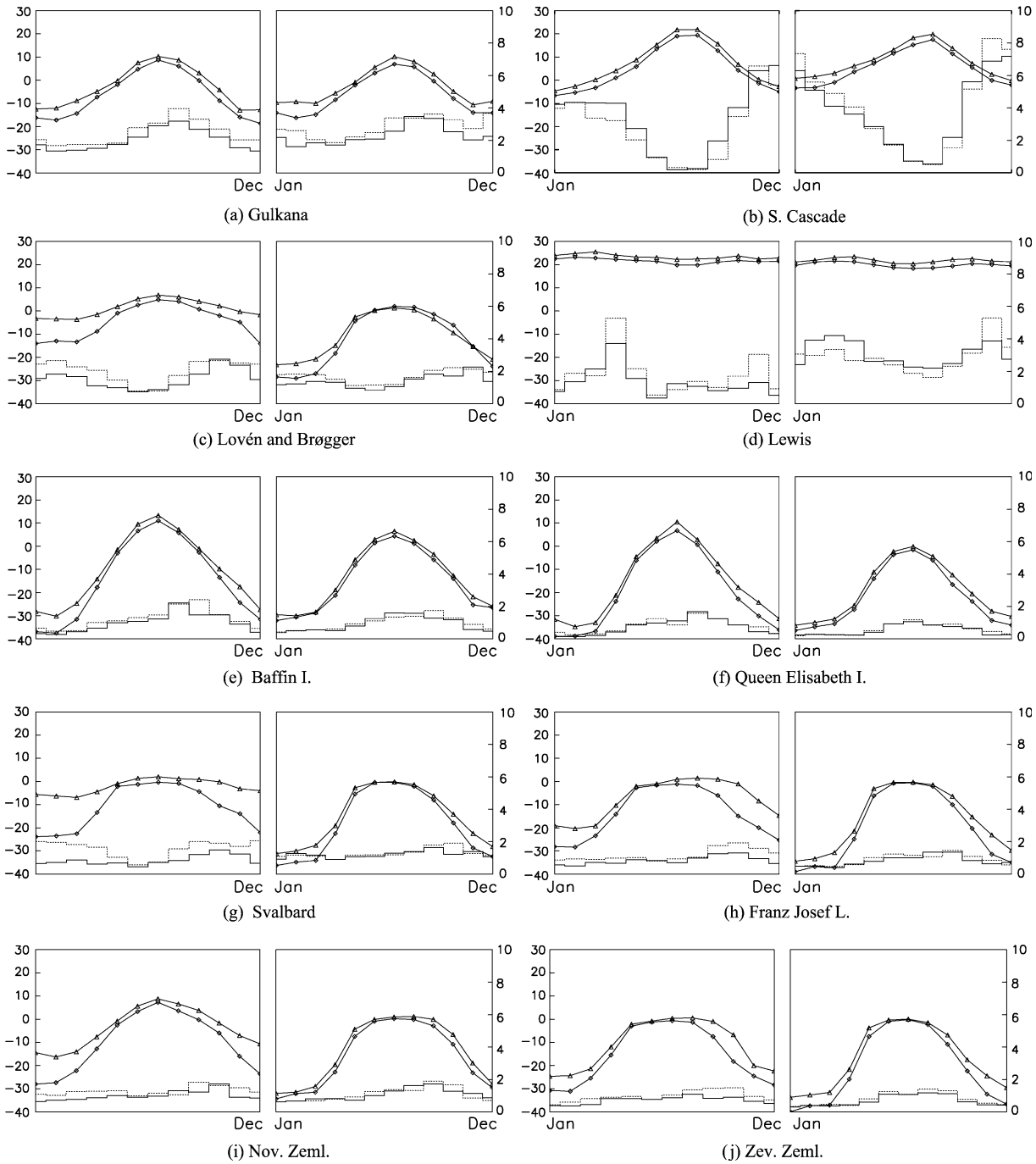

Fig. 2 (*continued*)

for the surrounding area, only the difference between the modelled present day temperature and the modelled $2 \times CO_2$ temperature at the corresponding grid points is used in this study.

The known pattern of larger temperature increase in high arctic regions in winter and small increase in summer emerges from both climate projections, however, the ECHAM result shows a considerably larger increase than the CCSR prediction. Since this pattern is connected to the sea ice cycle, the difference in the predictions seem to be connected to different predictions of the sea ice cycle.

The differences between the two modelled temperatures and amounts of precipitation for present and $2 \times CO_2$ time slice experiments are not very systematic for the different regions. Temperatures generally agree better than precipitation, although the annual pattern and total of the precipitation agree better than the monthly values.

4.2. Mass balance modelling

The mass balance model of Hock (1999) was applied to all of the 17 chosen glaciers and 6 glacierized areas. The applied parameters (melt factors, radiation coefficient, temperature and precipitation lapse rates) are listed in Table 1. These parameters are calibrated for each glacier individually. Unfortunately, no clear pattern emerged that allows to estimate the parameters based on the climatic situation of a glacier. This is especially true for the melt factor and radiation coefficient in the melt model and indicates missing physics in the simplified melt model.

Table 2
Overview over the mass balance results for several glaciers and larger, heavily glaciated regions

Glacier	CTRL	ECHAM $2 \times CO_2$ daily (mwe)	ECHAM $2 \times CO_2$ monthly (mwe)	CCSR $2 \times CO_2$ monthly (mwe)
1 Arolla	−0.45	−1.87	−1.87	−0.52
2 Gries	−0.21	−1.83	−1.84	−1.56
3 Stor	−0.03	−1.23	−1.05	−1.03
4 Enga	0.77	−2.80	−2.81	−1.81
5 Dzhankuat	−0.03	−1.75	−1.79	−1.19
6 Obruchev	−0.20	−1.85	−1.93	−1.75
7 Abramov	0.16	−1.22	−1.52	−0.43
8 No. 1	−0.19	−0.76	−0.90	−0.49
9 Aktru	0.06	−1.01	−1.18	−0.40
10 Shumsky	−0.23	−0.82	−0.77	−0.33
11 No. 31	0.07	−1.07	−1.08	−0.84
12 Wolverine	−0.18	−2.56	−2.51	−2.50
13 Gulkana	−0.32	−0.95	−0.73	−0.69
14 S. Cascade	−0.62	−2.87	−2.58	−2.10
15 M. Lovén	−0.31	−0.89	−1.10	−0.11
16 A. Brøgger	−0.41	−1.07	−1.31	−0.18
17 Lewis	−0.66	−2.01	−1.71	−1.95
Region	**CTRL**	**ECHAM $2 \times CO_2$ daily (mwe)**	**ECHAM $2 \times CO_2$ monthly (mwe)**	**CCSR $2 \times CO_2$ monthly (mwe)**
A Baffin I.	−0.23	−0.59	−0.59	−0.39
B Queen Elisabeth I.	−0.08	−0.30	−0.30	−0.18
C Svalbard	−0.52	−1.39	−2.01	−0.57
D Franz Josef L.	−0.11	−0.37	−0.18	−0.20
E Nov. Zeml.	−0.11	−0.27	−0.27	−0.53
F Zev. Zeml.	−0.08	−0.30	−0.30	−0.26

The mass balance for the CTRL situation corresponds to the mean specific mass balance for the current conditions (the mean of several years of mass balance, wherever such information was available). The mass balance for the larger regions corresponds to estimates by Dowdeswell et al. (1997).

The mass balance model was tuned to measured mass balances with respect to the net balance as well as to the melt and accumulation. Not only the absolute values were used but also the altitudinal distribution of the balance. With this tuning, a good agreement between measurements and model results is found as can be seen in Fig. 3.

The sensitivities found for the glaciers are in good agreement with values reported by Oerlemans and Fortuin (1992) and Braithwaite and Zhang (2000). Oerlemans and Fortuin (1992) suggest a global sensitivity of -0.4 mwe a^{-1} °C^{-1}, whereas Braithwaite and Zhang (2000) report values of -0.7 to -0.9 mwe a^{-1} °C^{-1}. The sensitivities found with Hock's mass balance model for this sample of glaciers range from -0.2 to -1.5 mwe a^{-1} °C^{-1}, with a mean of -0.6 mwe a^{-1} °C^{-1}. Higher values correspond to glaciers in a more maritime climatic setting while the smaller values correspond to glaciers in a more continental climatic setting. The wider range of sensitivities compared to the sensitivities of Braithwaite and Zhang (2000) can be explained by the varying climatic setting for this sample of glaciers. The sensitivity for Griesgletscher (Switzerland) is -0.64 mwe a^{-1} °C^{-1} compared to -0.69 mwe a^{-1} °C^{-1} from Braithwaite and Zhang (2000).

The results of the mass balance model are given in Table 2 for different climate scenarios: for the present conditions (control run CTRL), and for the projected $2 \times CO_2$ scenario ($2 \times CO_2$) obtained from the ECHAM and CCSR climate models (Fig. 2). The influence of averaging was tested with the ECHAM model for which either daily cycles or only monthly means of the air temperature were considered. The projected net mass balances for different glaciers differ, however, for 8 of the glaciers, this difference is smaller than 10% and the largest difference is 25%. The differences of the mass balances for the different climate models are larger and the CCSR model generally gives a smaller reduction of the mass balance than the ECHAM model.

The results from the mass balance modelling based on the climate model scenarios are unambiguous: due to a strong temperature increase in each of these

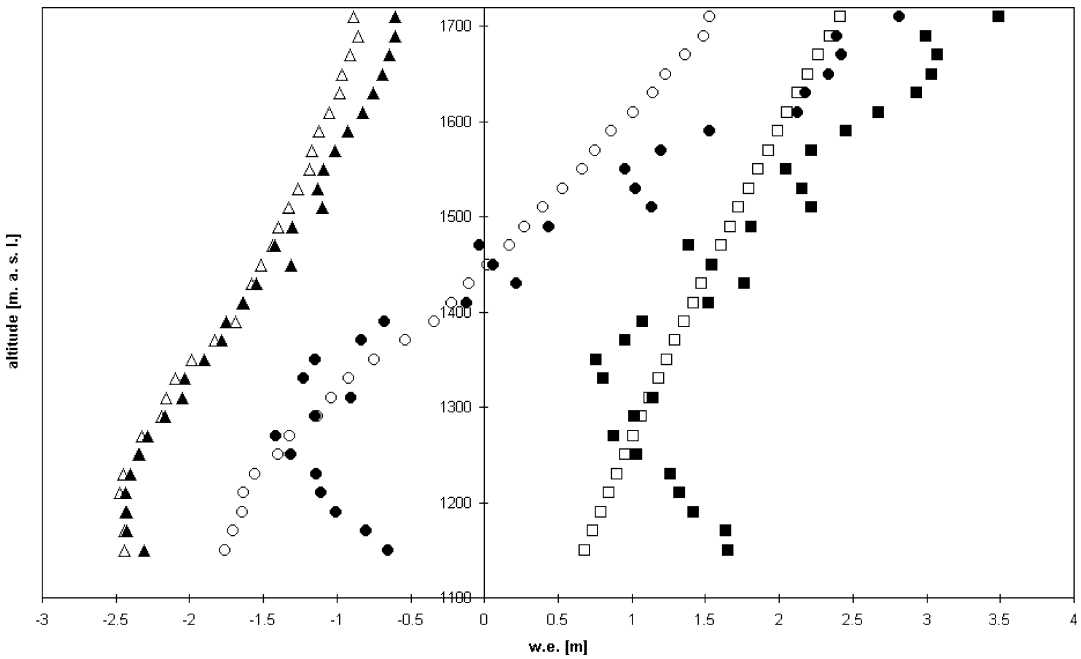

Fig. 3. Comparison of the measured and modelled altitudinal mass balance distribution for Storglaciären. Filled icons correspond to the measured values, the empty icons correspond to the modelled ones. The specific net mass balance is shown in circles, the melt in triangles, and the accumulation in squares, correspondingly. The correlation between the measured and the modelled net balance is 0.95.

regions, the mass balances of all of the considered glaciers will become strongly negative and all glaciers will start to retreat considerably in the near future. Glaciers in more maritime climatic conditions generally will experience a more pronounced change (e.g. South Cascade Glacier, Engabreen) than glaciers in continental conditions (e.g. Glacier No. 1, Gulkana Glacier, Storglaciären). This signal is not clearly visible and it may be hidden in other signals of processes which determine the sensitivity of glaciers. Of course, if the elevation range of the mean equilibrium line comes close to the elevation range of the surrounding topography, a large portion of the ice surface becomes ablation zone and the glacier will disappear.

The heavily glacierized areas in the high Arctic show a relatively small reduction in net mass balance (Dowdeswell et al., 1997). This is due to the generally low temperatures in these areas, even under $2 \times CO_2$ conditions. However, this change is still important, because of the large surface area of the high latitude glaciers and ice caps (Table 2).

4.3. Dynamic response of glaciers

The modelled mass balances were used as boundary conditions for the modelling of the glacier dynamics. The mass balance conditions were linearly interpolated between the CTRL conditions and the $2 \times CO_2$ conditions for each grid cell.

Table 3 and Fig. 4 show the projected volume change between present day and 2050 for 11 of the 17 glaciers, for which the bed topography is known. The rate factor in the glacier flow model was kept constant at a value of 0.07 a^{-1} bar^{-3} for all glaciers, which corresponds to temperate glacier ice (Albrecht, 1999; Vieli, 1996; Hubbard et al., 1998; Gudmundsson, 1994). The flow model was run without basal sliding since information or estimates of basal sliding are difficult to obtain and not available for most glaciers. Direct measurements are rare and indirect methods require additional information on basal conditions and assumptions on the relation between these conditions and basal sliding. (van der Veen, 1999). Omission of sliding may lead to inaccuracies in the distribution of ice thickness and velocities, however, an integral quantity such as ice volume is still quite accurate (Albrecht, 1999).

The effect of the feedback between glacier geometry and mass balance was tested using the following approach: a first model run used a mass balance evolution obtained from a linear interpolation between present day mass balance and $2 \times CO_2$ mass balance, both computed for

Table 3
Glacier volume evolution for the case study glaciers

Glacier	Volume (10^6 m^3)	Dynamical change			Static change	
		Step 1 (%)	Step 2 (%)	Step 3 (%)	Stat. Dyn. (%)	Static (%)
1 Arolla	289.7	−73.8	−77.4	−77.6	−48.1	−61.3
2 Gries	390.0	−55.6	−60.1	−60.6	−53.5	−70.0
3 Stor	291.9	−28.3	−31.0	−31.3	−38.7	−33.5
5 Dzhankuat	111.9	−41.6	−39.4	−39.8	−87.3	−100.0
6 Obruchev	71.7	−48.6	−55.4	−57.5	−70.4	−100.0
8 No. 1	109.1	−46.5	−54.1	−64.5	−31.3	−59.1
9 Aktru[a]	592.5	−8.5			−52.2	−60.3
10 Shumsky	162.0	−45.1	−52.6	−52.6	−31.3	−65.0
11 No. 31	186.7	−45.4	−49.3	−49.8	−53.8	−61.1
14 S. Cascade	164.5	−77.4	−79.4	−79.9	−59.4	−80.2
17 Lewis	6.1	−100.0	−100.0	−100.0	−100.0	−100.0

Percentual changes relative to the original volume are given for the three iteration steps as well as to simpler volume evolution estimates. The simpler estimates were obtained by (a) asuming a constant glacier surface area (static) and (b) using a statistical relation between glacier surface and volume to determine the hypothetical glacier shrinkage due to the mass loss given by the mass balance.

[a] Due to numerical stability problems, the program was only run with a simpler code, using a shallow ice approximation.

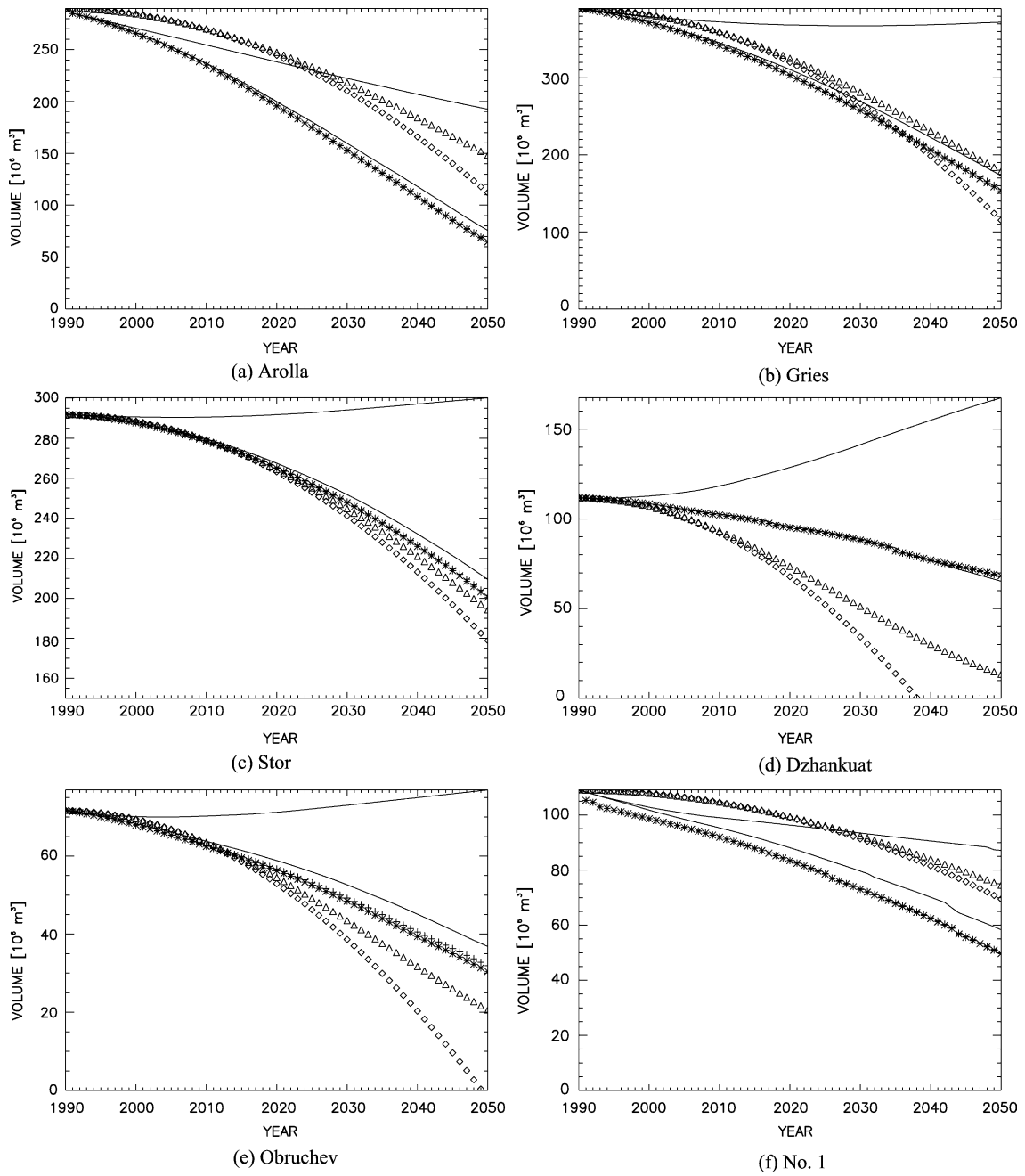

Fig. 4. Volume evolution of the modelled glaciers. Three iteration steps proofed to be enough to reach a state where the mass balance–surface elevation feedback almost vanished. In addition to the three iterations are two more simpler estimates of volume evolution: the first, with assuming constant glacier surface area (static) and the second taking into account the reduction of surface area by volume loss through a statistical relationship. The upper solid line shows the result of the integrations using the CTRL mass balance throughout the whole period. The lower solid line shows the first iteration step: mass balance for the CTRL and $2 \times CO_2$ situation based on the current topography is linearly interpolated over the whole time period and used input for the dynamics model. (+) show the second iteration step, where the $2 \times CO_2$ mass balance is recalculated based on the final topography from iteration one. ($*$) is the third iteration that is performed in analogy to the second one. Triangles show a simpler estimate based on the statistical relationship while diamonds show the estimate with constant glacier surface area.

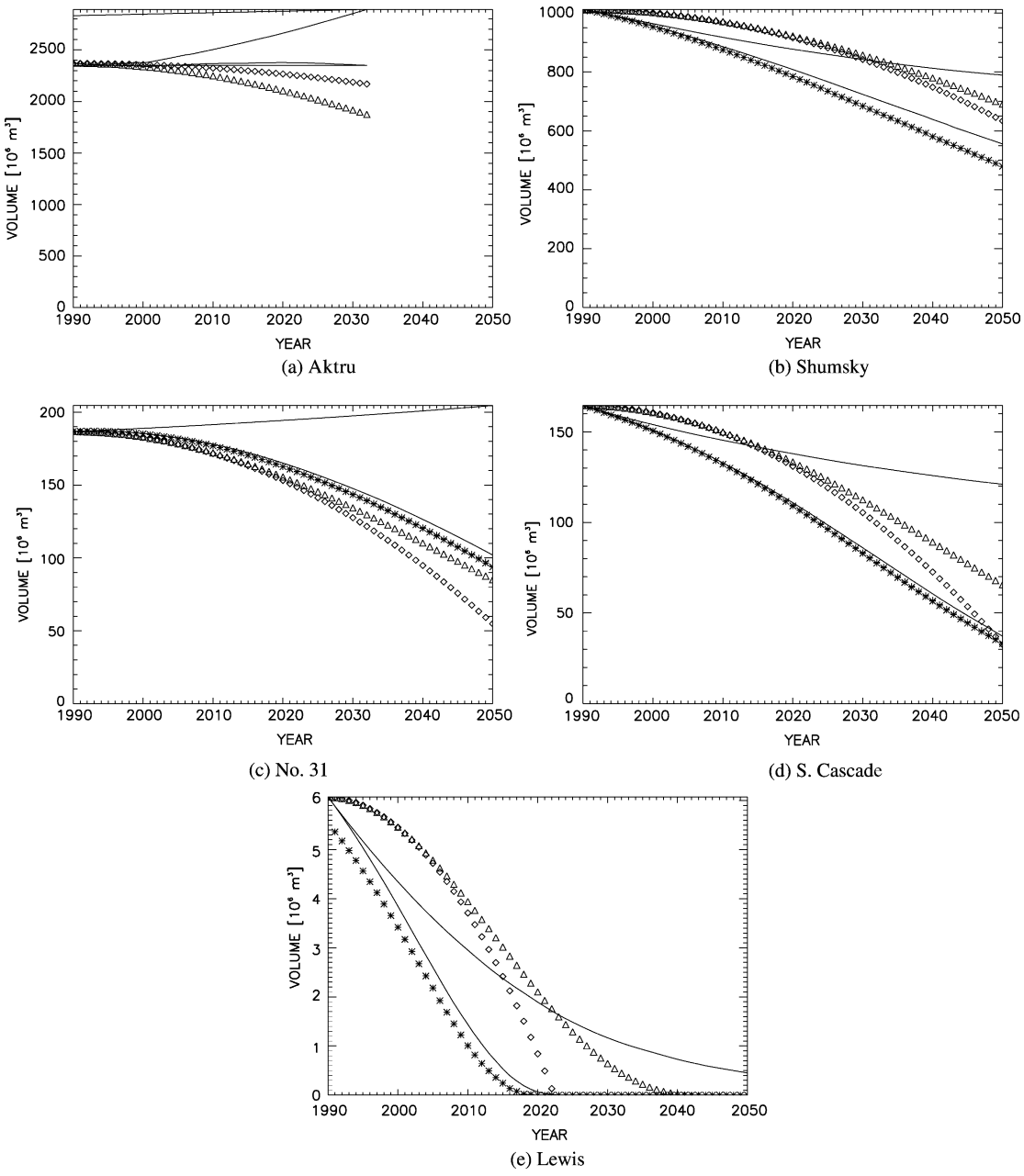

Fig. 4 (*continued*)

the present day glacier surface. At the end of that run, the glacier surface usually changed significantly. This new glacier surface was used for iteration. A new mass balance for the $2 \times CO_2$ situation was computed using the new surface computed for 2050. The glacier surface evolution was then recalculated using a interpolation between present day mass balance and the new $2 \times CO_2$ mass balance. This results in a larger mass loss in the second iteration step because the glacier surface

was lowered, and thus the mass balance becomes more negative due to higher melt. However, the changes between the second and third iteration step were always negligibly small.

However, for much longer modelling periods, surface area and surface topography for mass balance computations may need more frequent updates.

For most glaciers, bed topography is not known and the glacier flow model cannot be applied. A rough estimate of the future volume change can be made by neglecting ice flow and surface change altogether, and integrate the mass balance for the entire period on the initial ice surface. This static model leads to an overestimation of the volume reduction since mass loss is computed for a too large ice surface area if a glacier is shrinking. For the modelled glaciers, volume changes from the dynamic modelling can differ from those of static modelling by up to 60% (Table 3).

A third possibility is the use of a statistical relation between glacier surface and glacier volume as suggested by Bahr et al. (1997) to simulate the glacier dynamics for a given mass balance scenario. Compared to the results with a physical glacier flow model, these statistical relation produces different results in both directions (Table 3). The final mass change is either overestimated or underestimated, depending on how a particular glacier fits into the statistics. The method may be applicable, despite the large scatter, if the modelled sample of glaciers is large enough and if only the total sum of all volume changes is required, e.g. to estimate the contribution of glaciers and ice caps to sea level changes.

4.4. GCM comparison

The difference between the two GCM simulations is surprisingly small. Global annual mean temperature for the present situation is 5.6 °C for the ECHAM and 2.5 °C for the CCSR, the corresponding values for the $2 \times CO_2$ case are 7.7 and 4.2 °C. The temperature increase is 2.1 °C for the ECHAM and 1.7 °C for the CCSR. Similarly the agreement for the precipitation: the ECHAM yields an annual global mean precipitation of 817 mm/yr for the present situation and 851 mm/yr for the $2 \times CO_2$ scenario (an increase of 34 mm/yr), while the corresponding values for the CCSR are 793 and 830 mm/yr (an increase of 37 mm/yr). On a local basis there is good agreement between the projected temperature change from both models. However, there is a substantial disagreement concerning the precipitation (Fig. 2). But the influence of the precipitation on glacier mass balance is small. To compensate for an increase in temperature of 1 K, a precipitation increase of 30–40% is necessary (Oerlemans et al., 1998). The most significant difference arises for the two glaciers in Svalbard (Midtre Lovénbreen and Austre Brøggerbreen). This may be caused by a substantial difference in sea ice extent in the two climate models. A pronounced shrinkage of the sea ice extent causes large changes in the ECHAM $2 \times CO_2$ scenario, while this is not so drastic in the CCSR $2 \times CO_2$ simulation.

Table 4
Comparison of mass balance results obtained from scenarios from both the ECHAM4 and the CCSR

Glacier	CTRL (10^6 m^3)	CCSR		ECHAM	
		(10^6 m^3)	(%)	(10^6 m^3)	(%)
Arolla	289.6	99.6	−65.6	75.9	−73.8
No.31	186.7	119.0	−36.3	100.1	−46.4
S. Cascade	164.5	59.1	−64.1	41.9	−74.5
Lewis	6.1	0.0	−100.0	0.0	−100.0

Please note that these runs were performed based on model output of monthly mean values of temperature and precipitation, thus no daily cycle was implemented.

The small differences in mass balances also result in small differences in the volume development. The volume evolution of four glaciers (Arolla, South Cascade, Lewis, No. 31) was calculated using the mass balance scenarios obtained from the climate scenarios of both GCM's. The results are shown in Table 4 and in Fig. 5.

The different volume decreases of each of these four glaciers match to within approximately 10% for the two different predictions of the ECHAM and CCSR climate models.

5. Discussion and conclusions

The combined use of a climate forecast provided by a GCM, a glacier mass balance model and a glacier

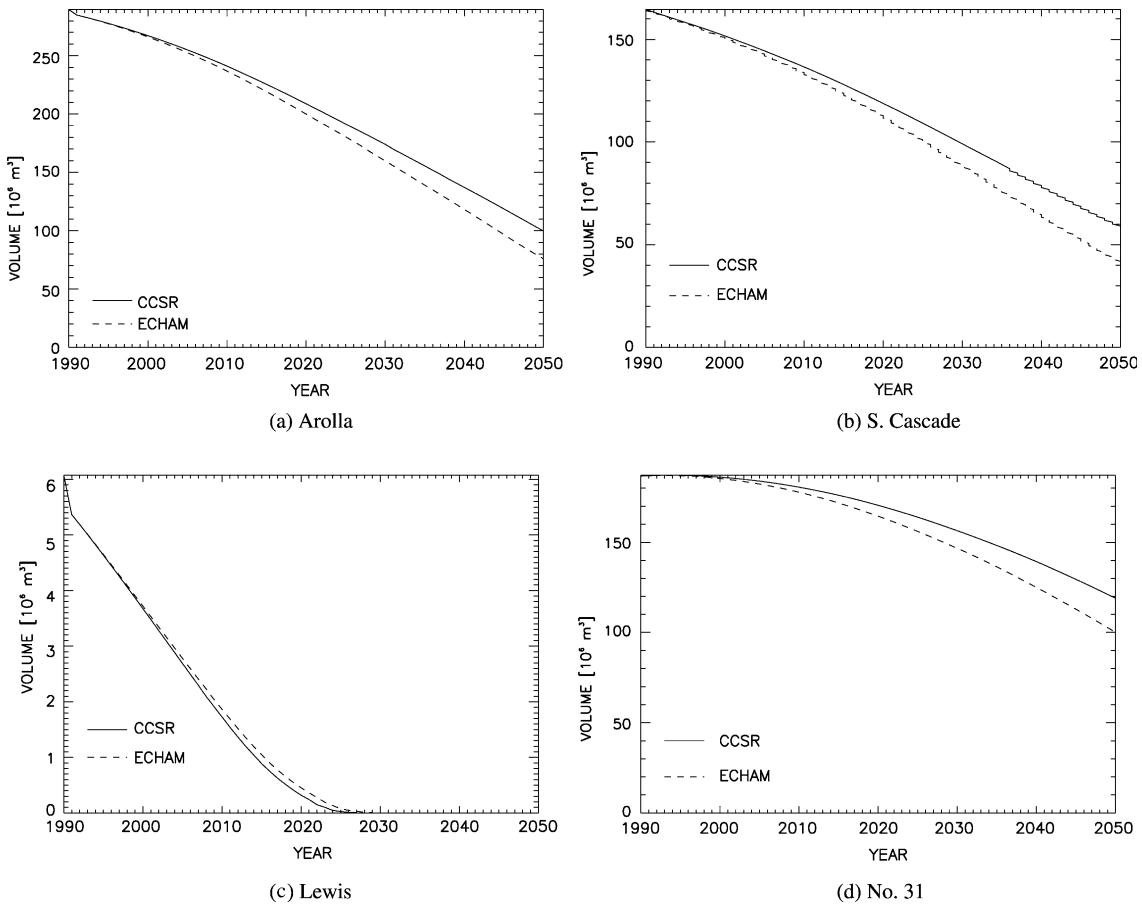

Fig. 5. Volume development of four glaciers showing the influence of the different GCM scenarios.

flow model is a logical step towards the prediction of the future evolution of glaciers and their potential contribution to water resources planning and to sea level changes. Under these conditions, the prediction of the evolution of integral quantities such as the total ice volume of a glacier is reliable for a few decades up to a century, provided that the prediction of the climatic conditions is reliable. According to the predictions of two different climate models (ECHAM4 and CCSR climate model), the temperature is found to increase strongly during the winter months, but it also shows a warming during the transition from spring to summer, and again between summer and fall, thus extending the melt season by three to four weeks. The two GCMs show a good agreement in the possible change of temperature. The change in precipitation, however, differs strongly. But this change is of minor importance since a realistic precipitation change affects mass balance much less than realistic changes in temperature.

As a consequence, all modelled glaciers suffer a substantial retreat within the coming 50 years in the enhanced greenhouse climate. This pattern results with both climate projections (the ECHAM4 T106 and the Tokyo T106 time slice model runs with doubling CO_2 in 2050). The difference resulting from the use of different GCMs can be substantial, however, the results of both models were consistent (i.e. the resulting change in mass balance is always of the same sign) and the difference probably has a comparable magnitude as the uncertainty of the mass balance measurements itself. Another important point

is the fact that the use of different emission scenarios in the GCM will lead to significantly different climate projections.

The projected warming leads to a strong reduction in mass balance and thus a significant volume loss. This loss can for a single glacier only be assessed accurately by using a dynamic model. Comparison with simpler estimates shows considerable discrepancies. A static approach yields to a general overestimation of the volume loss, while an approach using a statistical relation between glacier surface area and glacier volume yields differences in both directions. Therefore, if a large enough sample of glaciers is selected, this approach may be suitable for estimates of the total sum of volume changes (e.g. for sea level changes). The mass loss is larger for smaller glaciers in the lower regions, compared to the larger, heavily glaciated areas in the arctic (Svalbard, Severnaya Zemlya, Novaya Zemlya, Franz Josef Land, Baffin Island, Ellesmere Island). Nevertheless, due to the large extent of these areas, this contribution is not negligible.

Acknowledgements

We thank A. Ohmura, ETH Zürich, for stimulating discussions. Regine Hock, Stockholm University, provided a former version of the mass balance model and O. Albrecht, ETH Zürich, developed part of the glacier model.

This work was initiated and partly funded by the Alliance for Global Sustainability, a partnership of the Massachusetts Institute of Technology, University of Tokyo and the Swiss Federal Institute of Technology, grants no. 2-85207-97 and ETH grant no. 0-20690-99. The Swiss Scientific Computing Center generously provided the necessary computer resources for the time slice experiment with the ECHAM climate model. This study is supported by the National Center for Competence in Climate Research (NCCR Climate) funded by the Swiss National Science Foundation.

The digital elevation model (DEM) of Abramov glacier was kindly provided by F. Pertziger (SANIGMI). R.M. Krimmel (USGS) kindly provided the DEM, bed topography and climate data of S. Cascade glacier, information for Gulkana glacier came from R.S. March (USGS), and those of Wolverine from B. Kennedy (USGS). The DEM of Engabreen was obtained from the NVE. The DEM's of the two glaciers from Svalbard were kindly provided by NPI. S. Hastenrath provided with reports and additional information on Lewis glacier.

References

Aellen, M., Funk, M., 1988. Massenbilanz des Griesgletschers von 1961 bis 1986. Vergleich verschiedener Bestimmungsverfahren. In: Vischer, D. (Ed.), Schnee, Eis und Wasser alpiner Gletscher, vol. 94. Mitteilungen der Versuchsanstalt für Wasserbau, Hydrologie und Glaziologie der ETH Zürich, pp. 9–50.

Albrecht, O., 1999. Dynamics of glacier and ice sheets: a numerical model study. PhD thesis, ETH Zürich, Switzerland, no. 13278.

Albrecht, O., Jansson, P., Blatter, H., 2000. Modelling glacier response to measured mass balance forcing. Ann. Glaciol. 31, 91–96.

Bahr, D.B., Meier, M.F., Peckham, S.D., 1997. The physical basis of glacier volume–area scaling. J. Geophys. Res. 102 (B9), 20355–20362.

Blatter, H., 1995. Velocity and stress fields in grounded glaciers: a simple algorithm for including deviatoric stress gradients. J. Glaciol. 41 (138), 333–344.

Braithwaite, R.J., Zhang, Y., 2000. Sensitivity of mass balance of five swiss glaciers to temperature changes assessed by tuning a degree-day model. J. Glaciol. 46 (152), 7–14.

Cao, M.S., 1998. Detection of abrupt changes in glacier mass balance in the Tien Shan Mountains. J. Glaciol. 44 (147), 352–358.

Chaohai, L., Tianding, H., 1992. Relation between recent glacier variations and climate in the Tien Shan mountains, central Asia. Ann. Glaciol. 16, 11–20.

Cherkasov, P.A., Nikitin, S.A., 1989. Glaciers, Snow Cover and Avalanches in the Mountains of Kazhakstan, Chapter On the method of volume calculation of mountain Glaciers from data of ground and airborne radiolocation surveys, on the example of the Djungarski Alatau, Nakau, Almaty, Kazhakstan, pp. 18–37 (in Kussian).

Cherkasov, P.A., Ahmetova, G.S., Hastenrath, S., 1996. Ice flow and mass continuity of shumsky glacier in the djungarski alatau range of Kazakhstan, central Asia. J. Geophys. Res. 101 (D8), 12913–12920.

Colinge, J., Blatter, H., 1998. Stress and velocity fields in glaciers. Part I. Finite difference schemes for higher-order glacier models. J. Glaciol. 44, 448–456.

Cubasch, U., Waszkewitz, J., Hegerl, G.C., Perlwitz, J., 1995. Regional climate changes as simulated in time-slice experiments. Clim. Change 31, 273–304.

Cubasch, U., Caneill, J.Y., Filiberti, M.A., Hegerl, G., Johns, T.C., Keen, A., Parey, S., Thual, O., Ulbrich, U., Voss, R., Waszkewitz, J., Wild, M., Ypersele, J.P., 1997. Anthropogenic

Climate Change. European Commission, Office for official Publications of the EU, Luxemburg.

Dowdeswell, J.A., Hagen, J.O., Björnsson, H., Glazovsky, A.F., Harrison, W.D., Holmlund, P., Jania, J., Koerner, R.M., Lefauconnier, B., Ommanney, C.S.L., Thomas, R.H., 1997. The mass balance of circum-arctic glaciers and recent climate change. Quat. Res. 48, 1–14.

Emori, S., Nozawa, T., Abe-Ouchi, A., Numaguti, A., Kimoto, M., Nakajima, T., 1999. Coupled ocean-atmosphere model experiments of future climate change with an explicit representation of sulfate aerosol scattering. J. Met. Soc. Jpn 77, 1299–1307.

Fountain, A.G., Jacobel, R.W., 1997. Advances in ice radar studies of a temperate alpine glacier, South Cascade Glacier, Washington, USA. Ann. Glaciol. 24, 303–308.

Funk, M., Morelli, R., Stahel, W., 1997. Mass balance of Griesgletscher 1961–1994: different methods of determination. Z. Gletscherk. Glazialgeol. 33 (1), 41–56.

Garnier, B., Ohmura, A., 1968. A method of calculating the direct shortwave radiation income on slopes. J. Appl. Meteorol. 7, 796–800.

Gates, W.L., 1992. AMIP: the atmospheric model intercomparison project. Bull. Am. Meteorol. Soc. 73, 1962–1970.

Gudmundsson, G.H., 1994. Convergent Glacier Flow and Perfect Sliding Over a Sinusoidal Bed. PhD thesis, ETH Zürich, no. 10711.

Haeberli, W., Boesch, H., Scherler, K., Østrem, G., Wallén, C.C., 1989. World Glacier Inventory. Status 1988. IAHS (ICSI)-UNEP-UNESCO, pp. 408.

Hagen, J.O., Liestøl, O., 1990. Long-term glacier mass-balance investigations in svalbard, 1950–88. Ann. Glaciol. 14, 102–106.

Hastenrath, S., 1996. Glaciological studies on Mount Kenya 1691–1996 Technical report, Department of Atmospheric and Oceanic Sciences, University of Wisconsin, Madison.

Hock, R., 1999. A distributed temperature-index ice- and snowmelt model including potential direct solar radiation. J. Glaciol. 45 (149), 101–111.

Hodge, S.M., Trabant, D.C., Krimmel, R.M., Heinrichs, T.A., March, R.S., Josberger, E.G., 1998. Climate variations and changes in mass of three glaciers in western north america. J. Clim. 11 (9), 2161–2179.

Holmlund, P., 1996. Maps of Storglaciären and their use in glacier monitoring studies. Geogr. Ann. 78A (2/3), 193–196.

Holmlund, P., Jansson, P., 1999. The Tarfala mass balance programme. Geogr. Ann. 81A (4), 621–631.

Hubbard, A., Blatter, H., Nienow, P., Mair, D., Hubbard, B., 1998. Comparison of a three dimensional model for glacier flow with field data from Haut Glacier d'Arolla, Switzerland. J. Glaciol. 44 (147), 368–378.

IASH(ICSI)-UNEP-UNESCO, 1988. In: Haeberli, W., Muller, P. (Eds.), Fluctuations of Glaciers (FOG) 1980–1985, vol. V. World Glacier Monitoring Service, Paris, p. 290.

IASH(ICSI)-UNEP-UNESCO, 1991. In: Haeberli, W., Herren, E. (Eds.), Glacier Mass Balance Bulletin (GMB). Bulletin No. 1 (1988–1989). World Glacier Monitoring Service, p. 70.

IASH(ICSI)-UNEP-UNESCO, 1993. In: Haeberli, W., Muller, P. (Eds.), Fluctuations of Glaciers (FOG) 1985–1990, vol. VI. World Glacier Monitoring Service, Zurich, pp. 322, plus plates.

IASH(ICSI)-UNEP-UNESCO, 1993. In: Haeberli, W., Herren, E. (Eds.), Glacier Mass Balance Bulletin (GMB). Bulletin No. 2 (1990–1991). World Glacier Monitoring Service, p. 67.

IASH(ICSI)-UNEP-UNESCO, 1994. In: Haeberli, W., Hoelzle, M., Bösch, H. (Eds.), Glacier Mass Balance Bulletin (GMB). Bulletin No. 3 (1992–1993). World Glacier Monitoring Service, p. 80.

IASH(ICSI)-UNEP-UNESCO, 1996. In: Haeberli, W., Hoelzle, M., Suter, S. (Eds.), Glacier Mass Balance Bulletin (GMB). Bulletin No. 4 (1994–1995). World Glacier Monitoring Service, p. 90.

IASH(ICSI)-UNEP-UNESCO, 1998. In: Haeberli, W., Muller, P. (Eds.), Fluctuations of Glaciers (FOG) 1990–1995, vol. VII. World Glacier Monitoring Service, Zurich, p. 298.

IASH(ICSI)-UNEP-UNESCO, 1999. In: Haeberli, W., Hoelzle, M., Frauenfelder, R. (Eds.), Glacier Mass Balance Bulletin (GMB). Bulletin No. 5 (1996–1997). World Glacier Monitoring Service, p. 96.

IASH(ICSI)-UNESCO, 1967. In: Kasser, P., (Ed.), Fluctuations of Glaciers (FOG) 1959–1965, vol. I. Permanent Service on the Fluctuations of Glaciers of the IUGG-FAGS, p. 52.

IASH(ICSI)-UNESCO, 1973. In: Kasser, P., (Ed.), Fluctuations of Glaciers (FOG) 1965–1970, vol. II. Permanent Service on the Fluctuations of Glaciers of the IUGG-FAGS, p. 357.

IASH(ICSI)-UNESCO, 1977. In: Müller, F., (Ed.), Fluctuations of Glaciers (FOG) 1970–1975, vol. III. Permanent Service on the Fluctuations of Glaciers of the IUGG-FAGS, p. 269.

IASH(ICSI)-UNESCO, 1985. In: Haeberli, W. (Ed.), Fluctuations of Glaciers (FOG) 1975–1980, vol. IV. World Glacier Monitoring Service, Paris, p. 265.

IPCC, 1990. Climate Change, the IPCC Scientific Assessment. Cambridge University Press, Cambridge, pp. 200.

Jania, J., Hagen, J.O. (Eds.), 1996. Mass Balance of Arctic Glaciers. International Arctic Science Committee, Working Group on Arctic Glaciology IASC Report No. 5.

Johannesson, T., Raymond, C., Waddington, E., 1989. Time-scale for adjustment of glaciers to changes in mass balance. J. Glaciol. 35 (121), 355–369.

Kääb, A., 1996. Photogrammetrische Analyse zur Früherkennung gletscher- und permafrostbedingter Naturgefahren im Hochgebirge Mitteilungen der Versuchsanstalt für Wasserbau, Hydrologie und Glaziologie der ETH Zürich, 145, pp. 182.

Kjøllmoen, B. (Ed.), 2000. Glasiologiske undersøkelser i Norge 1999, pp. 144, Norges vassdragsog energidirektorat.

Kotlyakov, V.M., 1997. World Atlas of Snow and Ice Resources Russian Academy of Sciences. Institute of Geography, Moscow.

March, R.S., 2000. Mass balance, meteorological, ice motion, surface altitude, runoff and ice thickness data at Gulkana Glacier, Alaska, 1995 balance year Water Resources Investigations Report 00-4074, US Geological Survey.

Oerlemans, J., Fortuin, J.P.F., 1992. Sensitivity of glaciers and small ice caps to Greenhouse warming. Science 258, 115–117.

Oerlemans, J., Anderson, B., Hubbard, A., Huybrechts, P., Jóhannesson, T., Knap, W.H., Schmeits, M., Stroeven, A.P., van de

Wal, R., Wallinga, J., Zuo, Z., 1998. Modelling the response of glaciers to climate warming. Clim. Dyn. 14, 267–274.

Ohmura, A., 2001. Physical basis for the temperature-based melt-index method. J. Appl. Meteorol. 40 (4), 753–761.

Ohmura, A., Wild, M., Bengtsson, L., 1996. A possible change in mass balance of Greenland and Antarctic ice sheets in the coming century. J. Clim. 9 (9), 2124–2135.

Ostenson, N.A., Sellman, P.V., Péwé, T.L., 1965. The bottom topography of Gulkana Glacier, Alaska Range, Alaska. J. Glaciol. 5 (41), 652–660.

Pertziger, F.I. (Ed.), 1996. Abramov Glacier Data Reference Book: Climate, Runoff, Mass Balance. Technical University, Munich.

Roeckner, E., Arpe, K., Bengtsson, L., Christoph, M., Claussen, M., Dümenil, L., Esch, M., Giorgetta, M., Schlese, U., Schulzweida, U., 1996. The Atmospheric General Circulation Model ECHAM4: Model Description and Simulation of Present Day Climate, vol. 218. Max Planck Institute for Meterology, pp. 171.

Roeckner, E., Bengtsson, L., Feichter, J., Lelieveld, J., Rodhe, H., 1999. Transient climate change simulations with a coupled atmosphere–ocean GCM including the tropospheric sulfur cycle. J. Clim. 12 (10), 3003–3032.

Schneeberger, C., Albrecht, O., Blatter, H., Wild, M., Hock, R., 2001. Modelling the response of glaciers to a doubling in atmospheric CO_2: a case study on Storglaciären, northern Sweden. Clim. Dyn. 17 (11), 825–834.

Sharp, M., Richards, K.S., Arnolds, N., Willis, I.C., Nienow, P., Tison, J., 1993. Geometry, bed topography, and the drainage system structure of Haut Glacier d'Arolla, Switzerland. Earth Surf. Processes Landforms 18 (6), 557–571.

van der Veen, C.J., 1999. Fundamentals of Glacier Dynamics. Balkema, Rotterdam.

Vieli, A., 1996. Modellierung der Veränderung des Griesgletschers seit 1961 und Perspektiven für die Zukunft. Diploma Thesis. ETH Zürich.

Wild, M., Calanca, P., Scherrer, S.C., Ohmura, A., 2003. Effects of polar ice sheets on global sea level in high-resolution greenhouse scenarios . J. Geophys. Res. 108(05), 4165, doi:10.1029/2002JD002451.

Wild, M., Ohmura, A., Cubasch, U., 1997. GCM simulated surface energy fluxes in climate change experiments. J. Clim. 10, 3093–3110.

Zhang, X., Zhu, G., Qian, S., Cheng, J., Shen, Y., 1985. Radar measuring ice thickness of no. 1 glacier at the source of urumqi river, Tianshan. J. Glaciol. Geocryol. 7 (2), 123–132 (in Chinese).